Version: 06.09.2023

Thermal behavior of silver-gold core-shell nanocubes: *In-situ* X-ray diffraction and *in-situ* electron microscopy (SEM, TEM)

A. Karatzia[1], K. Loza[1], O. Prymak[1], M. Heggen[2], and M. Epple[1,*]

[1] Inorganic Chemistry and Center for Nanointegration Duisburg-Essen (CeNIDE), University of Duisburg-Essen, Universitaetsstr. 5-7, 45141 Essen, Germany;

e-mail matthias.epple@uni-due.de

[2] Ernst Ruska-Centre for Microscopy and Spectroscopy with Electrons, Forschungszentrum Jülich GmbH, 52425 Jülich, Germany

Abstract

Silver-gold core-shell nanocubes were prepared by adding a gold layer on the surface of silver nanocube seeds. The bimetallic nanocubes contained silver and gold in a molar ratio of 3 : 1 and were stabilized by poly(N-vinylpyrrolidon) (PVP). To elucidate their thermal behavior, silver nanocubes and silver-gold core-shell nanocubes (both 90 nm edge length) were studied *in-situ* by *in-situ* scanning electron microscopy (SEM), *in-situ* transmission electron microscopy (TEM), and *in-situ* X-ray powder diffraction (XRD) up to 800 °C. The nanocubes got rounded edges at 600 °C. Above 700 °C, they started to sublime under the low-pressure conditions (10^{-5} to 10^{-3} Pa) of the *in-situ* experiments. Core-shell Ag@Au nanocubes showed a similar behavior, but diffusion of gold into the silver core was observed above 400 °C, leading to pore-filling and alloying with the silver core. After sublimation of silver, sintered gold remained. The sublimation was due to the enhanced vapor pressure of nanoscopic silver in comparison to microscopic silver or bulk silver as control experiments clearly showed. Notably, all structural changes occurred well below the melting temperatures of silver and gold, i.e. in the solid state.

Keywords

Silver; gold; nanoparticles; X-ray diffraction; electron microscopy; in-situ experiments

Introduction

Nanoparticles of noble metals like gold, silver, and platinum are of interest because they have different properties compared to their corresponding bulk material. They have special physicochemical properties due to their small size and high specific surface area which make them attractive in different areas like biomedicine, catalysis, optics, and electronics.[1-5] In bimetallic nanoparticles, the properties of the individual components can be combined to realize new properties due to synergetic effects of the two metals that can be tuned by variation of composition and shape.[6, 7] In heterogeneous catalysis, variation of particle composition, size and shape can enhance selectivity, efficiency, and stability for a given reaction. Faceted particles with well-defined shape provide special sites for reactant adsorption and reaction intermediates which can enhance the catalytic activity.[8-13] Catalytic reactions often occur at elevated temperatures which may change the properties of the nanoparticles. However, due to their high specific surface area, their thermal behavior is different from the corresponding bulk materials.[14, 15] For instance, nanoparticles tend to melt or sublime at lower temperature compared to their corresponding bulk materials.[16-18] From a thermodynamic point of view, the sublimation temperature of nanoparticles decreases with decreasing particle size according to the Kelvin equation.[18]

To study their thermal behavior, *in-situ* TEM studies have been performed on metallic nanoparticles of different size and shape.[19-21] Silver nanoparticles are particularly interesting because their sublimation temperature is low in comparison to other noble metals.[22, 23] The sublimation of silver nanocubes has been studied with *in-situ* TEM by Ding et al.[24] They found that the (110) surfaces exhibit greater stability compared to theoretical predictions[24] As far as the temperature-induced effects on bimetallic nanoparticles are concerned, much less is known.

Silver has a melting temperature of 962 °C, and gold has a melting temperature of 1064 °C. Both metals form mixed crystals. The alloy is called electrum.[25] A separation of both metals on the nanoscale is possible by the preparation of bimetallic nanoparticles where one metal acts as core and the second as shell. At elevated temperature, the mobility of the metal atoms will increase, and alloying is expected. Here we report on a comprehensive study by complementary *in-situ* methods, i.e. X-ray powder diffraction (XRD), scanning electron microscopy (SEM), and transmission electron microscopy (TEM) to assess the stability and crystallinity of silver and silver-gold core-shell nanocubes up to 1000 °C.

Materials and Methods

Chemicals

We used ethylene glycol (p.a.; Sigma-Aldrich), poly(N-vinylpyrrolidone) (PVP_{55}, M_w = 55,000 g mol^{-1}, Sigma-Aldrich), L(+)-ascorbic acid (p.a.; Carl Roth), silver nitrate (99%; Carl Roth), and silver powder (5-8 μm ≥99.9%; Sigma-Aldrich). An aqueous solution of tetrachloridoauric acid ($HAuCl_4$) was prepared by dissolution of gold powder (99.96%; Alfa Aesar) in *aqua regia*. All glassware was cleaned with boiling *aqua regia* and then with boiling water prior to use. Ultrapure water (Purelab Ultra instrument; ELGA) was used as solvent for all experiments and glassware cleaning procedures unless otherwise stated.

Nanoparticle Synthesis

Silver nanocubes (Ag nanocubes). A previously reported synthesis was modified.[26-29] In a typical synthesis, 6 mL ethylene glycol was heated to 160 °C for 1 h under air access. Then, 30 μL of a 0.1 M HCl solution was added to the heated solution. After 10 min, 3 mL of a solution of $AgNO_3$ (0.1 M) and 3 mL of a solution of PVP_{55} (0.1 M with respect to the monomer), both in ethylene glycol, were thoroughly mixed and then quickly added to the reaction solution. The reaction vessel was closed with a septum and stirred. Immediately after the addition, the solution gradually became transparent, then milky-white, then orange, and finally ochre/yellow/green. After 20 h stirring at 160 °C, the reaction was stopped by quenching to room temperature with an ice bath. The particles were isolated by centrifugation for 30 min at 14,200 rpm (22,190 g) and washed once with acetone and then twice with water. Finally, the nanocubes were redispersed in degassed water and stored under argon at 4 °C to prevent oxidation.[30]

Silver-gold core-shell nanocubes (Ag@Au nanocubes). 0.6 mg silver nanocubes were dispersed as seeds in 45 mL water. 1.2 mL of 0.1 M ascorbic acid was added as a weakly reducing agent. Next, the pH was adjusted to 12 with 1 M NaOH. 40 mL $HAuCl_4$ solution (0.06 mM) was added dropwise with a syringe pump at 0.15 mL min^{-1} under stirring. The reaction mixture was vigorously stirred for 1 h. The particles were collected by centrifugation (30 min at 22,190 g) and washed four times with water. The particles were redispersed in degassed water and stored at 4 °C under argon.

This ratio of silver to gold represents the optimum of a number of syntheses where the silver-gold ratio was systematically varied. Different ratios led to incomplete gold coating, galvanic dissolution of the silver nanoparticles, or inhomogeneous particle populations.

Analytical Methods

Ultraviolet-visible spectroscopy (UV-Vis) was carried out with a Varian Cary 300 instrument from 280 to 800 nm with background correction (water). Hydrodynamic particle diameter, zeta potential, and polydispersity index (PDI) were determined by dynamic light scattering (DLS) with a Malvern Zetasizer Nano ZS ZEN 3600 instrument.

Scanning electron microscopy (SEM) was performed with an Apreo S LoVac instrument (ThermoFisher Scientific). 10 µL of each dispersion was dropped onto a silicon wafer, dried at ambient temperature in air, and examined in high vacuum. Energy-dispersive X-ray spectroscopy (EDX; UltraDry EDS detector, ThermoFisher Scientific) was used for elemental analysis and to visualize the elemental distribution (mapping) of silver and gold in the core-shell nanoparticles. *In-situ* SEM studies were performed in the same instrument with a µ-heating sample holder (ThermoFisher Scientific). The sample was drop-cast on a silicon nitride MEMS chip and gradually heated to 1000 °C with a heating rate of 5 K min^{-1} under a pressure of 10^{-4} Pa.

Transmission electron microscopy (TEM) was performed with a FEI Titan microscope, equipped with a Cs-probe corrector (CEOS Company), operating at 300 kV at 10^{-5} Pa.[31] *In-situ* TEM was carried out with a TEM heating sample holder (Wildfire, DENS Solutions Company) and a nano-chip with carbon support.

The concentrations of silver and gold were determined by atomic absorption spectroscopy (AAS) with a Thermo Electron Corporation M-Series instrument. For the determination of silver, the silver content of the sample was dissolved in concentrated nitric acid, followed by dilution with water. For the determination of gold, the sample was dissolved in *aqua regia* and then diluted with water.

X-ray powder diffraction (XRD) was performed with a Bruker D8 Advance instrument in Bragg-Brentano geometry mode with Cu Kα radiation (λ = 1.54 Å; 40 kV, 40 mA) with a silicon single crystal sample holder to minimize background scattering. *In-situ* XRD was carried out on a Panalytical Empyrean instrument in Bragg-Brentano mode with Cu Kα radiation (40 kV, 40 mA), equipped with a high-temperature chamber HTK 16 (Anton Paar). For XRD, the batches of 7 to

10 syntheses were pooled and freeze-dried after previous quality control by DLS. The nanoparticles were mixed with microcrystalline LaB_6 (SRM 660b from NIST, a = 4.15689 Å) as reference material. The sample was deposited on a tantalum holder and investigated in high vacuum (10^{-3} Pa) from 25 to 800 °C with a heating rate of 5 K min^{-1} between the steps. After reaching each temperature, the temperature was kept constant for one hour to record one X-ray powder diffractogram.

Results and Discussion

Monometallic silver nanocubes served as cores for the preparation of bimetallic silver-gold core-shell nanocubes stabilized with poly(N-vinylpyrrolidone) (PVP). Silver nanoparticles have specific optical properties that can be assessed by UV-Vis spectroscopy. Figure 1 shows the major surface plasmon resonance (SPR) bands of the seeds, i.e. silver nanocubes, which are characteristic for their size and shape.[32, 33] The two bands at 461 and 518 nm are attributed to the quadrupole and dipole resonance mode, respectively.[34] The coating of the seeds with a gold shell led to a red-shifted maximum around 680 nm that is characteristic for gold nanoparticles.[35] The absence of the silver SPR band indicates the formation of a tight gold shell around the silver nanocubes.

Dynamic light scattering showed that both types of nanocubes were well dispersed and monodisperse with a narrow size distribution as indicated by the low polydispersity index (PDI). Their zeta potential was negative (-40 mV for silver nanocubes and -25 mV for silver-gold core-shell nanocubes) which indicates an electrosteric stabilization by PVP (Figure 1).

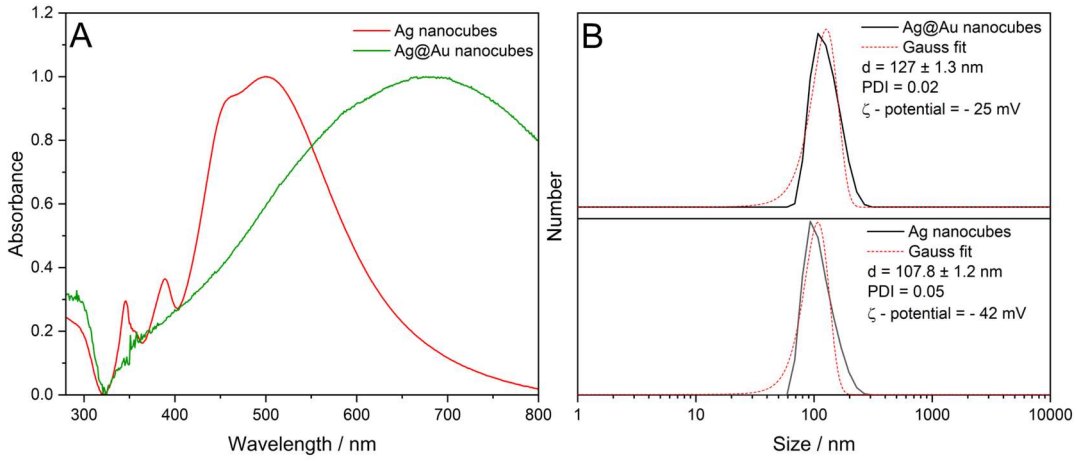

Figure 1. UV-Vis spectra (**A**) and dynamic light scattering results (**B**) of silver and silver-gold core-shell nanocubes. The particles are well dispersed in water. The replacement of the surface plasmon resonance of silver by that of gold indicates a tight gold layer around the silver core.

Scanning electron microscopy confirmed the formation of silver nanocubes as seeds (Figure 2). Silver nanocubes had an average edge length of 85±7 nm, and the bimetallic silver-gold core-shell nanocubes had an average edge length of 96±10 nm, in good agreement with the DLS results. The edges of the silver nanocubes were round as theoretically predicted.[36] The surface of the silver nanocubes was very smooth. After the deposition of gold on the surface of the silver nanocubes, the surface of the nanocubes became uneven due to the deposition of small gold nanoparticles which obviously did not form a smooth surface layer. However, UV-Vis spectroscopy (Figure 1) indicated that the gold shell was tight.

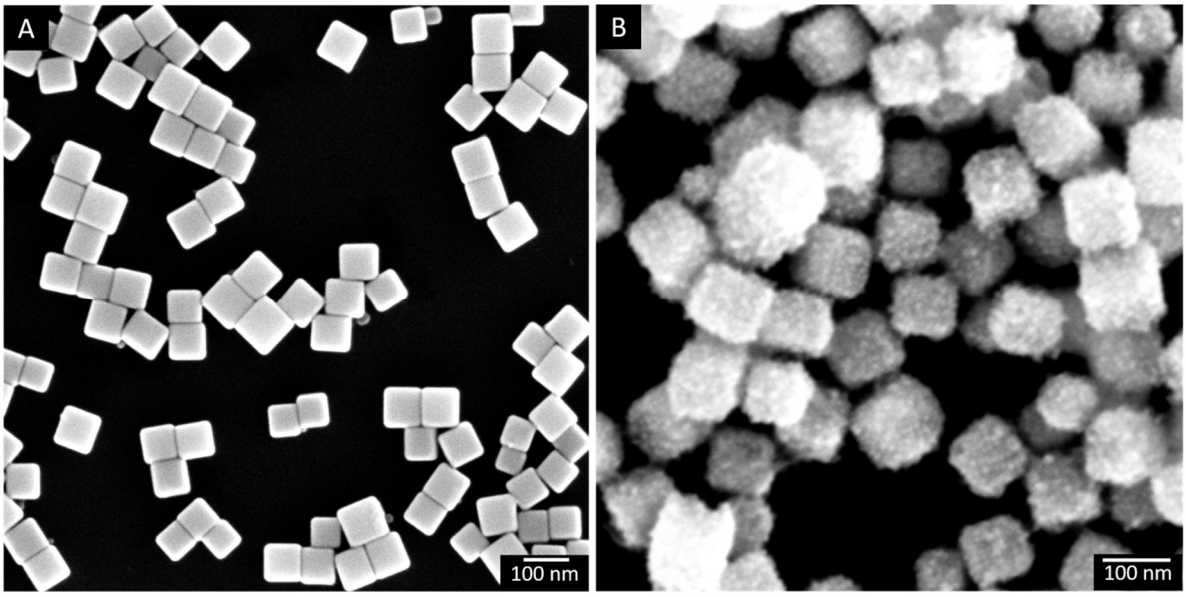

Figure 2. SEM images of silver nanocubes (**A**) and silver-gold core-shell nanocubes (**B**). Note the rough surface of the bimetallic nanocubes due to the irregular deposition of gold on the smooth silver surface.

Transmission electron microscopy (TEM) showed the silver nanocubes at higher magnification. Fast Fourier transformation (FFT) indicated the [001] orientation of the nanoparticle and their single-crystalline nature (Figure 3), in accordance with earlier studies.[27] X-ray powder diffraction

showed the characteristic peaks of metallic silver (fcc) accompanied by a very strong texture in the [200] direction as the nanocubes lay on their (100) faces.[27] Rietveld refinement gave a crystallite size of 90 nm, confirming the average cube edge length determined by electron microscopy, i.e. the silver nanocubes consisted of a single crystal.[27]

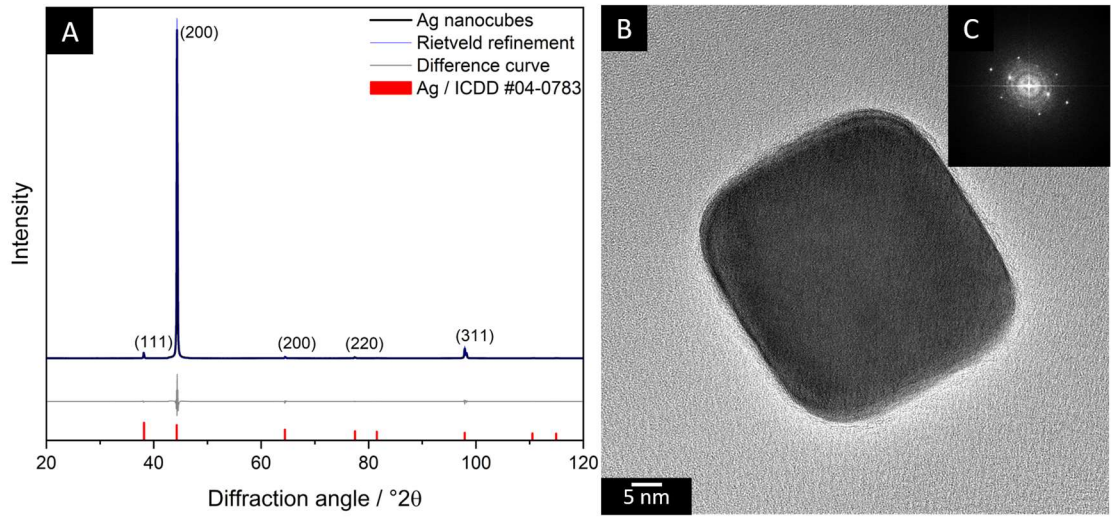

Figure 3. X-ray powder diffractogram with Rietveld refinement of silver nanocubes (**A**) and TEM image of a silver nanocube (**B**) with corresponding FFT analysis (**C**). The nanocubes show a strong preferred orientation and are single crystalline.

Figure 4 shows a TEM image of the surface of the silver-gold core-shell particles. The epitaxial on-growth of gold follows the Stranski-Krastanov mechanism, i.e. a layer-plus-island growth mode. The shell starts as a two-dimensional layer, but after reaching a critical thickness, 3D islands are formed.[37] XRD provided crystallographic information on the gold shell. Rietveld refinement gave a crystallite size of the gold particles of about 3 nm, i.e. about 1/3 of the particle size (10 nm) as seen in TEM. A similar behavior for the particle and crystallite size was found earlier for pentagonal twinned silver nanospheres.[38] The domain size of the silver core was about 70 nm, i.e. almost unchanged. The rough surface of the nanocubes strongly reduced the preferred orientation as the cubes did not lie flat on the (100) face.

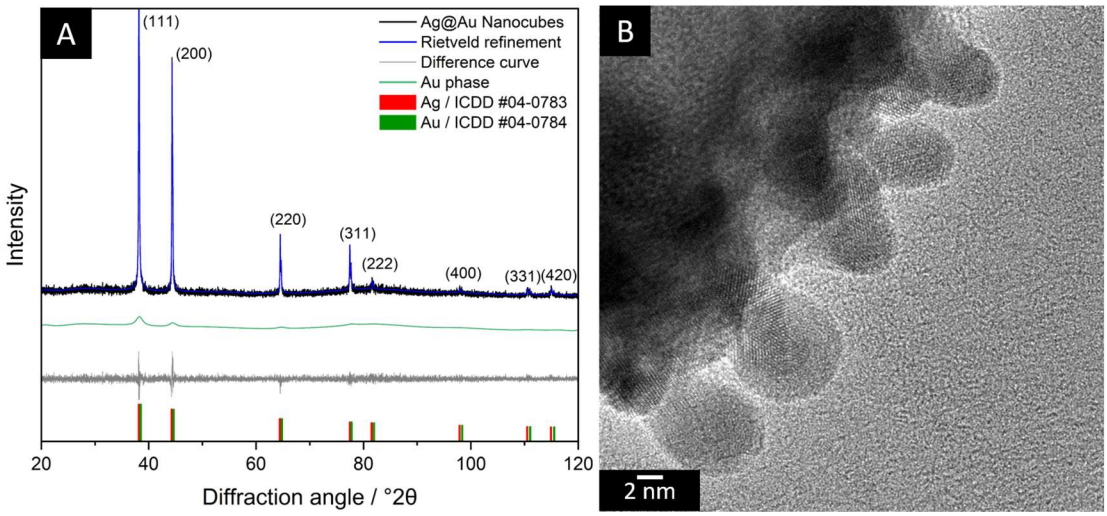

Figure 4. X-ray powder diffractogram of silver-gold core-shell nanocubes with Rietveld refinement (**A**) and TEM image of the edge of a silver-gold core-shell nanocube, showing the surface-nucleated gold particles (**B**). The preferred orientation of the nanocubes in XRD is considerably decreased due to the deposition of approximately spherical gold particles.

Energy-dispersive X-ray spectroscopy (EDX) was performed to analyze the local distribution of silver and gold in the bimetallic nanocubes and to determine the molar silver-to-gold ratio in the bimetallic nanocubes. EDX maps showed the core-shell nature of the bimetallic nanocubes, including the rough gold surface layer (Figure 5). The EDX results were validated by elemental analysis (AAS) and quantitative X-ray powder diffraction (Rietveld analysis), showing an excellent agreement of the three methods (Table 1). The molar ratio of silver to gold is about 3 : 1, i.e. the particles have an overall stoichiometry of Ag_3Au.

Table 1. Elemental composition of silver-gold core-shell nanocubes as determined by three independent methods, showing an approximate overall composition of Ag_3Au.

	AAS	**EDX**	**XRD**
Silver / mol%	77 ± 6	76 ± 4	72 ± 5
Gold / mol%	23 ± 7	24 ± 2	28 ± 5

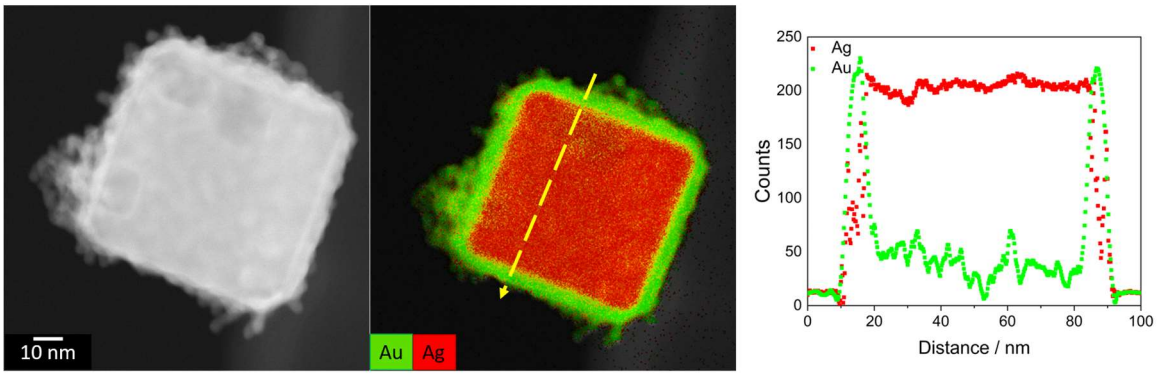

Figure 5. HAADF STEM and EDX map of a silver-gold core-shell nanocube and corresponding line scan (dashed yellow arrow) across the particle. The gold core is tight but becomes rougher towards the outside of the nanocube.

To observe thermal changes, *in-situ* electron microscopy and *in-situ* X-ray powder diffraction were carried out with silver nanocubes and silver-gold core-shell nanocubes. Both experiments were carried out in vacuum (10^{-5} to 10^{-3} Pa). *In-situ* transmission electron microscopy on silver nanocubes showed that they maintained their shape up to 600 °C when their corners became increasingly rounded. It has been reported that silver nanoparticles start to sublime in vacuum at 650 °C, depending on the pressure.[24] At and above 700 °C, the nanocubes lost their cubic shape and (110) faces were progressively exposed at the corners, leading to truncated octahedra. At 800 °C, the silver nanocubes had fully sublimed, leaving only pyrolysis products of the PVP and stretching marks on the carbon support of the sample holder (Figure 6).

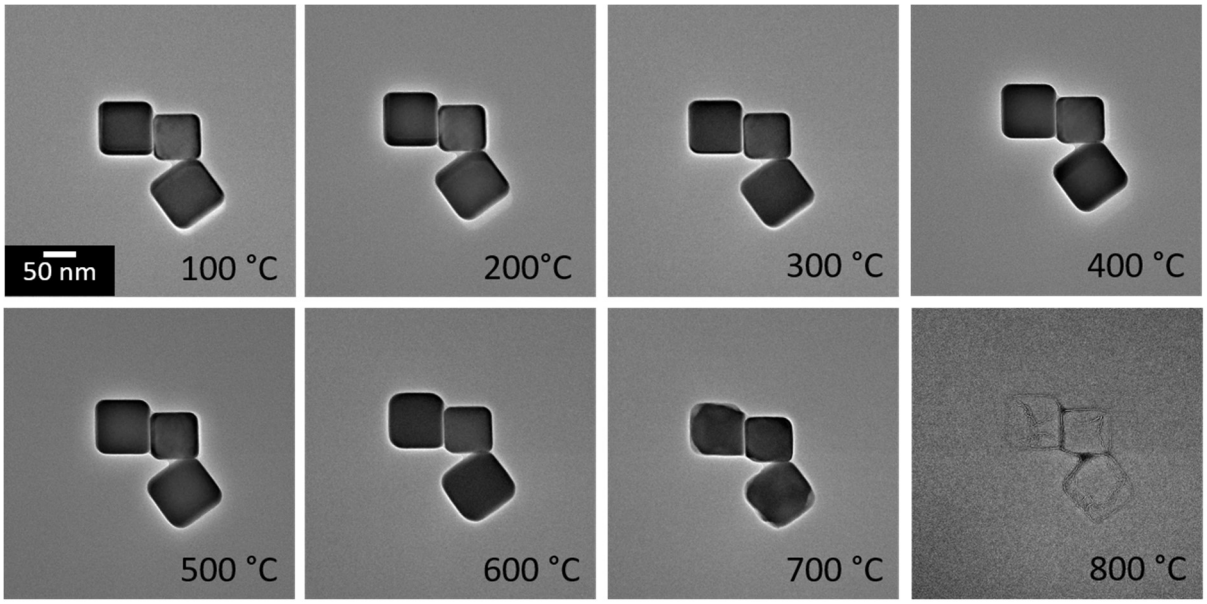

Figure 6. Bright-field TEM images of silver nanocubes during an *in-situ* heating experiment up to 800 °C. Above 700 °C, sublimation of silver started that was completed at 800° C (pressure 10^{-5} Pa) (see Supplementary Information for a corresponding video).

In-situ X-ray powder diffraction (Figure 7) showed the characteristic peaks of elemental silver, together with peaks of the tantalum sample holder and the reference compound LaB_6. With increasing temperature, the peaks shifted to lower 2θ values due to thermal expansion. Above 600 °C, the intensity of the diffraction peaks gradually decreased due to sublimation of silver.

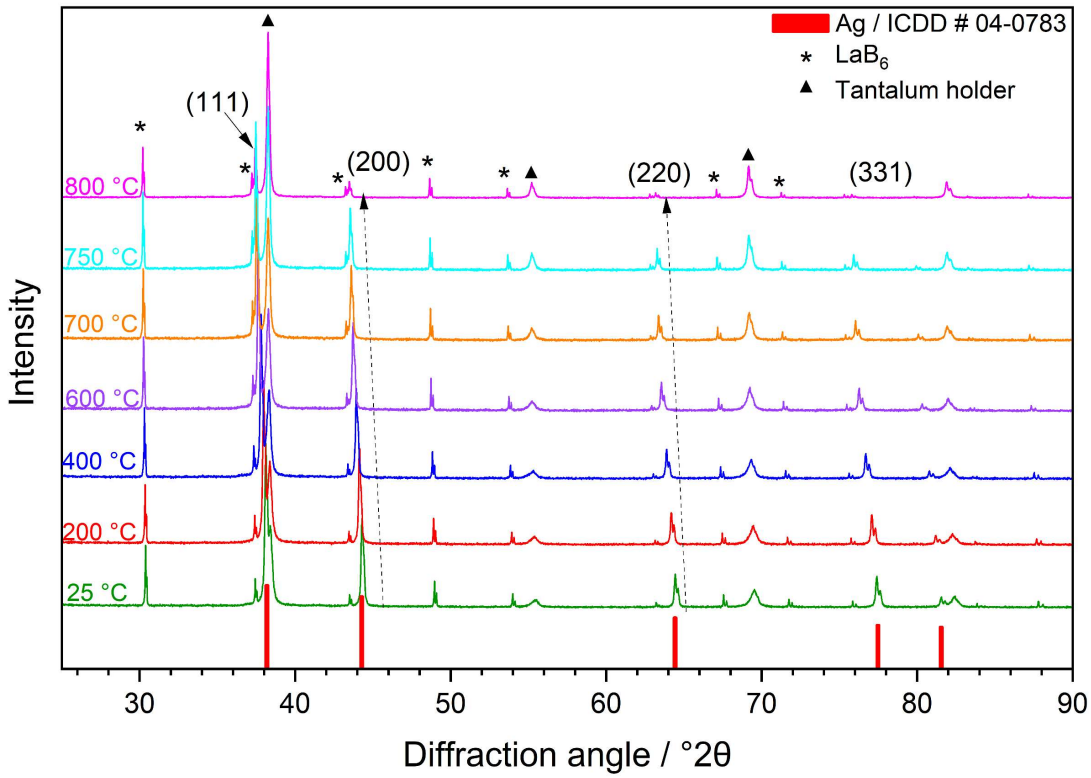

Figure 7. *In-situ* X-ray powder diffractograms of silver nanocubes mixed with LaB_6 standard (labelled with *; split peaks due Cu $K\alpha_{1,2}$ radiation) on a tantalum sample holder (labelled with ▲). The silver (fcc) peaks (111), (200), (220), and (331) are indicated. The peak shift to lower diffraction angles is due to thermal expansion. Above 600 °C, the peak intensity started to decrease due to sublimation (pressure 10^{-3} Pa). Note that the mixing of the silver nanocubes with LaB_6 considerably suppressed the texture (less preferred orientation of the nanocubes).

In-situ SEM experiments of silver-gold core-shell nanocubes (Figure 8) showed that above 400 °C, the nanocube surface became smoother and more uniform. Between 400 °C and 700 °C, gold diffused into the particle to form a nanoalloy. At 800 °C, silver had sublimed, and the remaining gold had formed a sintered shapeless particle. The EDX maps showed how the elements migrated with temperature and time, including alloy formation. Although the vapor pressure of solid gold is lower than that of solid silver, it has been noted that gold nanoparticles are more volatile than silver nanoparticles. This has been ascribed to surface melting in the case of gold which enhances

the vapor pressure.[39] It is well conceivable that such effects also during the heating of silver-gold core-shell nanocubes, especially if local alloying occurs. However, a quantitative understanding of all these connected effects is a very difficult task as thermodynamics (vapor pressure, melting, alloy formation), kinetics (sublimation and evaporation), and diffusion both in the solid state and the gas phase all need to be considered.

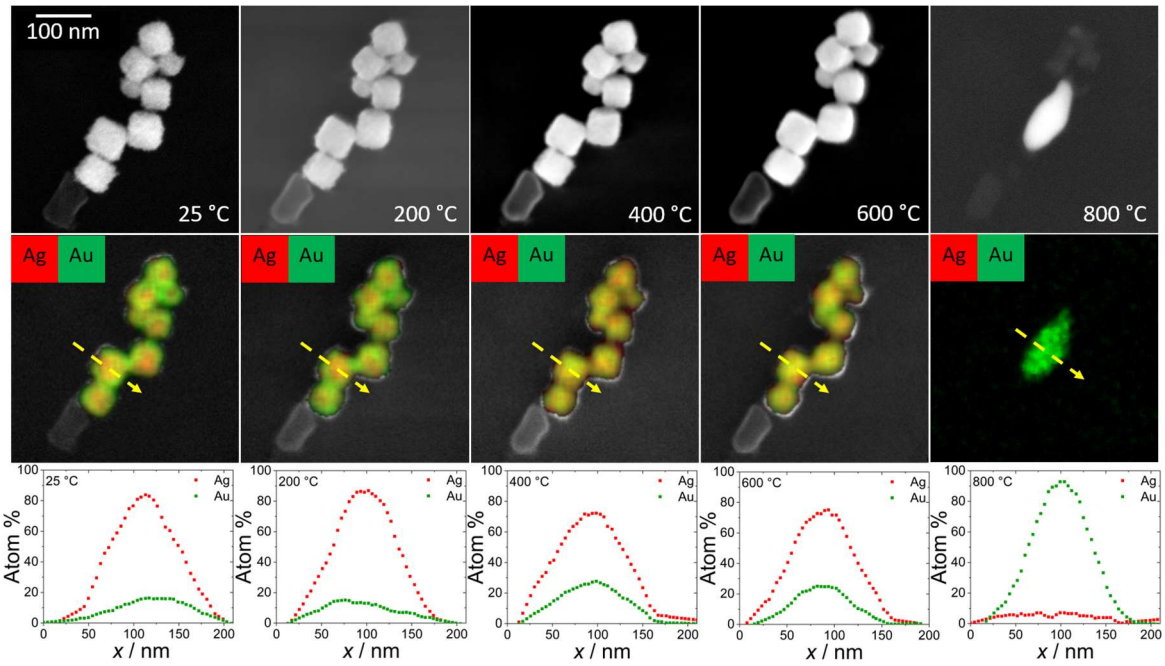

Figure 8. *In-situ* SEM images of silver-gold core-shell particles (**top row**), corresponding EDX maps (**center row**), and EDX line scans across one particle (**bottom row**). Above 400 °C, gold started to diffuse into the silver core. Above 600 °C, sublimation of silver started until only gold remained (see Supplementary Information for a corresponding video).

In-situ TEM experiments (Figure 9) showed pores inside the silver cubes caused by partial dissolution. These are due to galvanic replacement during the gold coating which cannot always be fully avoided.[40-42] Notably, they were absent in pure silver nanocubes (Figures 3 and 6). *In-situ* TEM (Figure 9) showed how they were filled between 400 and 500 °C by diffusion of gold into the silver core. As a result, the nanocubes were gradually converted from a core-shell structure to a nanoalloy. At 900 °C, the nanoparticles had lost their cubic shape and only gold remained after silver had sublimed (as confirmed by EDX).

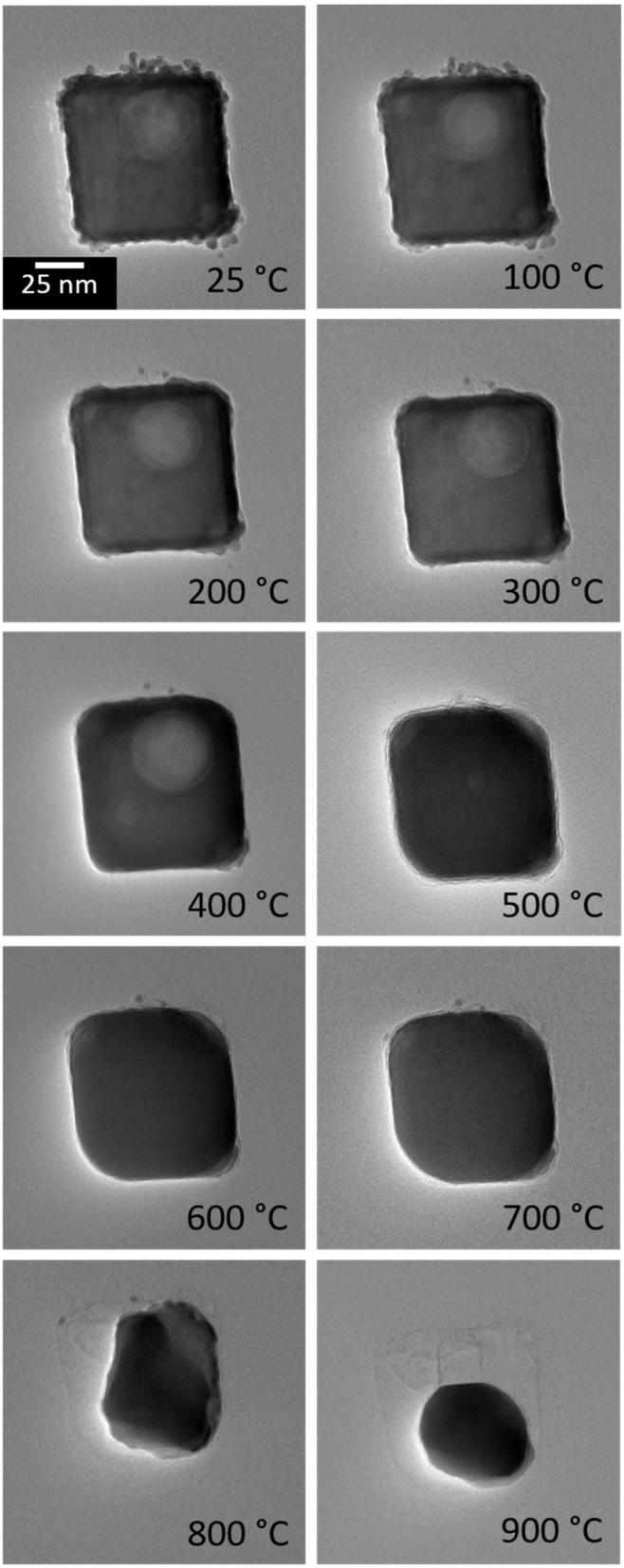
25 nm
25 °C
100 °C
200 °C
300 °C
400 °C
500 °C
600 °C
700 °C
800 °C
900 °C

Figure 9. Bright field *in-situ* TEM images of a silver-gold core-shell nanocube during heating. Note the presence of an internal pore in the nanocube formed by galvanic replacement during synthesis that was gradually filled with gold diffusing from the surface during the *in-situ* experiment above 400 °C (see Supplementary Information for a corresponding video).

Figures 10 and 11 show *in-situ* X-ray powder diffraction data of the silver-gold core-shell nanocubes in vacuum. Up to 600 °C the (200) and (220) peaks shifted to lower 2θ values due to thermal expansion. However, above 650 °C these peaks returned to higher 2θ values, and their intensity started to decrease. This shift confirms the alloying of silver and gold above 650 °C accompanied by lattice contraction. Gold has a smaller lattice constant (4.0786 Å) than silver (4.0862 Å),[43] but the lattice constants are so close that their diffraction peaks cannot be easily separated.[44] Above 650 °C, the peak intensity decreased due to silver sublimation. Unlike smaller alloyed AuAg nanoparticles (8 nm), the nanocubes did not undergo a structural relaxation due to recrystallization between 150 and 250 °C, pointing to well-separated phases of silver and gold in the core-shell nanoparticles.[41]

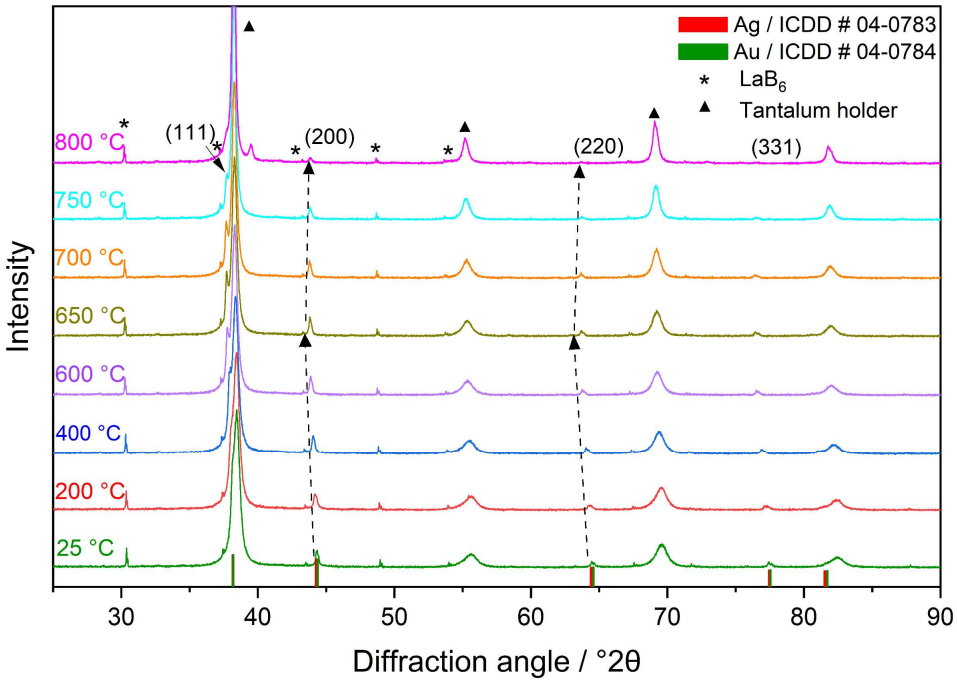

Figure 10. *In-situ* X-ray powder diffractograms of silver-gold core-shell nanocubes mixed with LaB_6 (labelled with *; split peaks due to Cu $K\alpha_{1,2}$ radiation)) on a tantalum sample holder (labelled with ▲). Miller indices of Ag and Au fcc phases are given in parentheses. The initial shift due to thermal expansion is reversed above 650 °C by gradual alloying of gold with silver.

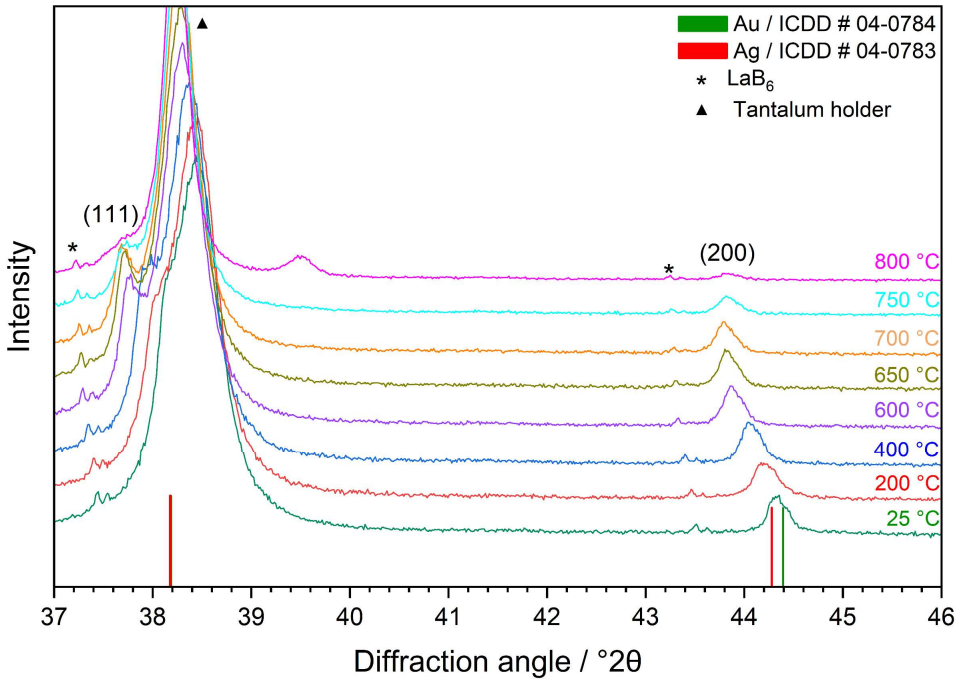

Figure 11. Enlargement of *in-situ* X-ray powder diffractograms from Figure 10, showing the (111) and (200) peaks of silver and gold.

Silver has a comparatively high vapor pressure compared to other noble metals (Ru, Rh, Pd, Os, Ir, Pt, and Au).[45] If silver nanoparticles are heated in vacuum, they undergo sublimation at even lower temperature compared to the bulk material due to their higher specific surface area and free enthalpy.[24, 46] Notably, the sublimation temperature of the nanoparticles deviates not only from the bulk material but also from microparticles: Nanoparticles begin to sublime at lower temperature.[23, 47] As confirmation we studied silver powder consisting of microparticles by *in-situ* X-ray powder diffraction (Figure 12). As the temperature increased, the silver peaks shifted due to thermal expansion. In contrast to silver nanocubes, the intensity of the peaks of the microparticles did not change with temperature, i.e. there was no sublimation of microparticles.

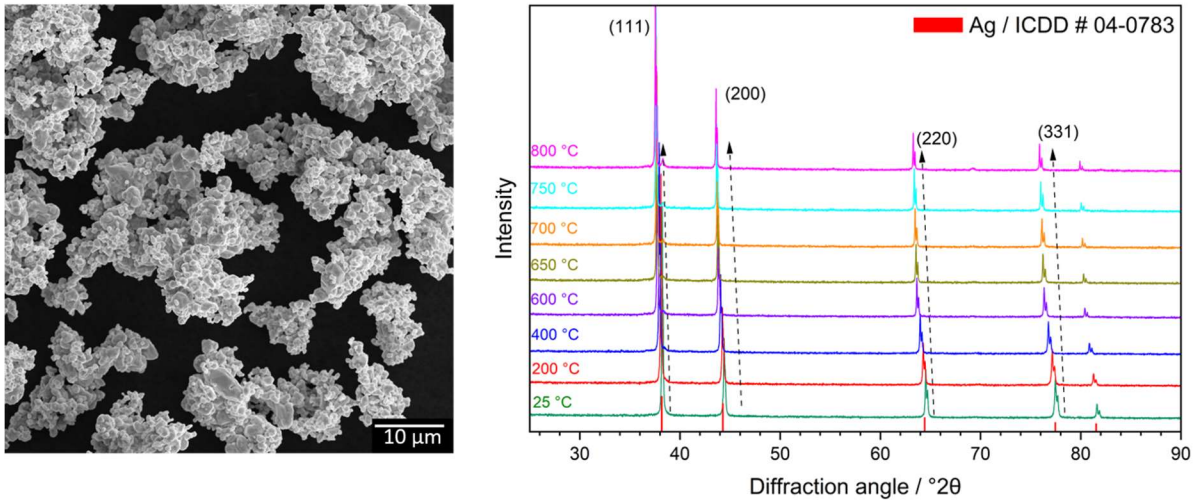

Figure 12. SEM image of silver microparticle powder (**left**). *In-situ* X-ray powder diffractometry of silver microparticle powder (**right**). Miller indices of the Ag fcc phase are indicated in parentheses. Silver microparticles show only the regular thermal shift and no indication for sublimation up to 800 °C.

Figure 13 shows the temperature dependence of the lattice parameter *a* of all investigated samples. Silver nanocubes and silver micropowder behaved as expected, matching very well with silver nanospheres (35 nm).[41] The silver-gold core-shell nanocubes initially had the same lattice parameter as the silver nanocubes but then showed a continuous deviation to lower lattice parameters indicating the diffusion of gold from the surface and the alloying with the silver core. Around 700 °C, a sudden drop of the lattice parameters of silver-gold core-shell nanocubes indicates that silver had sublimed and only gold had remained. The subsequent values closely matched those of pure gold nanoparticles (8 nm) which did not sublime under these conditions.[41]

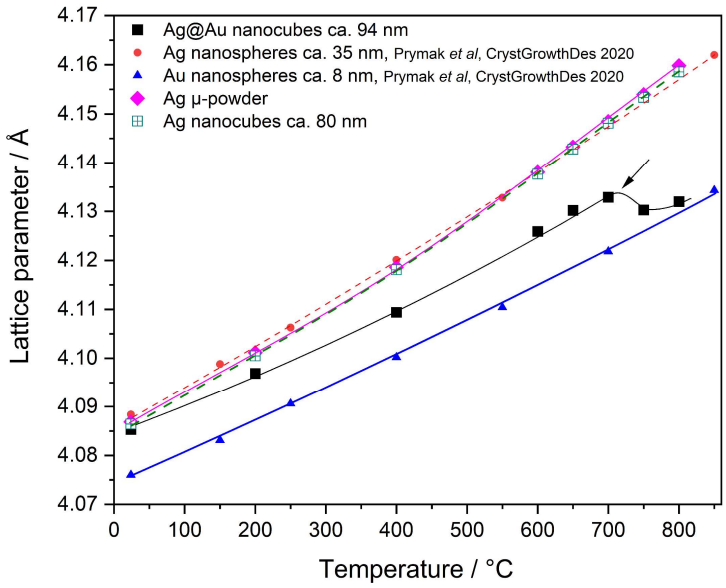

Figure 13. Temperature-dependent lattice parameter *a* of silver nanospheres (35 nm),[41] silver nanocubes, silver microparticles, silver-gold core-shell nanocubes, and gold nanospheres (8 nm).[41] The gradual alloying of gold into the silver leads to a continuous deviation for silver-gold core-shell nanocubes until at about 700 °C, silver sublimates and only gold remains.

Conclusions

In-situ electron microscopy and X-ray powder diffraction experiments showed that when silver nanocubes or gold-coated silver nanocubes are heated in vacuum, they maintain their shape and size up to 600 °C. Above 700 °C, silver starts to sublime in vacuum. In silver-gold core shell nanocubes, alloyed nanoparticles are formed above 400 °C due to diffusion of gold into the silver core as shown by EDX and XRD. Silver has a high vapor pressure, higher than that of gold and the other noble metals. However, the results clearly show that the sublimation of silver occurs only when nanoparticles are exposed to temperatures higher than 600 °C under vacuum. There is no indication for the presence of liquid phases, in accordance with the phase diagram, i.e. all observed processes occurred in the solid state. Overall, there is a remarkable degree of mobility of the constituting metal atoms in these core-shell nanoparticles.

Conflicts of Interest

The authors declare no conflict of interest.

Acknowledgments

We thank Mrs. Beate Römer and Mr. Robin Meya for elemental analyses.

Supplementary Material

The following videos of *in-situ* experiments are available as Supporting Information: Ag-Au core-shell nanocubes (TEM), Ag-Au core-shell nanocubes (SEM), Ag nanocubes (TEM).

References

1. Rodrigues, T. S.; da Silva, A. G. M.; Camargo, P. H. C., Nanocatalysis by noble metal nanoparticles: controlled synthesis for the optimization and understanding of activities. *J. Mater. Chem. A* **2019,** *7*, 5857-5874.
2. Pelaz, B.; Alexiou, C.; Alvarez-Puebla, R. A.; Alves, F.; Andrews, A. M.; Ashraf, S.; Balogh, L. P.; Ballerini, L.; Bestetti, A.; Brendel, C.; Bosi, S.; Carril, M.; Chan, W. C. W.; Chen, C.; Chen, X.; Chen, X.; Cheng, Z.; Cui, D.; Du, J.; Dullin, C.; Escudero, A.; Feliu, N.; Gao, M.; George, M.; Gogotsi, Y.; Grünweller, A.; Gu, Z.; Halas, N. J.; Hampp, N.; Hartmann, R. K.; Hersam, M. C.; Hunziker, P.; Jian, J.; Jiang, X.; Jungebluth, P.; Kadhiresan, P.; Kataoka, K.; Khademhosseini, A.; Kopecek, J.; Kotov, N. A.; Krug, H. F.; Lee, D. S.; Lehr, C. M.; Leong, K. W.; Liang, X. J.; Ling Lim, M.; Liz-Marzan, L. M.; Ma, X.; Macchiarini, P.; Meng, H.; Möhwald, H.; Mulvaney, P.; Nel, A. E.; Nie, S.; Nordlander, P.; Okano, T.; Oliveira, J.; Park, T. H.; Penner, R. M.; Prato, M.; Puntes, V.; Rotello, V. M.; Samarakoon, A.; Schaak, R. E.; Shen, Y.; Sjöqvist, S.; Skirtach, A. G.; Soliman, M. G.; Stevens, M. M.; Sung, H. W.; Tang, B. Z.; Tietze, R.; Udugama, B. N.; Van Epps, J. S.; Weil, T.; Weiss, P. S.; Willner, I.; Wu, Y.; Yang, L.; Yue, Z.; Zhang, Q.; Zhang, Q.; Zhang, X. E.; Zhao, Y.; Zhou, X.; Parak, W. J., Diverse applications of nanomedicine. *ACS Nano* **2017,** *11*, 2313-2381.
3. Jin, R., The impacts of nanotechnology on catalysis by precious metal nanoparticles. *Nanotechnol. Rev.* **2012,** *1*, 31-56.
4. Malekzad, H.; Sahandi Zangabad, P.; Mirshekari, H.; Karimi, M.; Hamblin, M. R., Noble metal nanoparticles in biosensors: recent studies and applications. *Nanotechnol. Rev.* **2017,** *6*, 301-329.
5. Azharuddin, M.; Zhu, G. H.; Das, D.; Ozgur, E.; Uzun, L.; Turner, A. P. F.; Patra, H. K., A repertoire of biomedical applications of noble metal nanoparticles. *Chem. Commun.* **2019,** *55*, 6964-6996.
6. Loza, K.; Heggen, M.; Epple, M., Synthesis, structure, properties, and applications of bimetallic nanoparticles of noble metals. *Adv. Funct. Mater.* **2020**, 1909260.
7. Dang-Bao, T.; Pla, D.; Favier, I.; Gomez, M., Bimetallic nanoparticles in alternative solvents for catalytic purposes. *Catalysts* **2017,** *7*, 207.
8. Zhang, T. J.; Walsh, A. G.; Yu, J. H.; Zhang, P., Single-atom alloy catalysts: structural analysis, electronic properties and catalytic activities. *Chem. Soc. Rev.* **2021,** *50*, 569-588.

9. Gao, C. B.; Lyu, F. L.; Yin, Y. D., Encapsulated metal nanoparticles for catalysis. *Chem. Rev.* **2021,** *121*, 834-881.
10. Du, Y. X.; Sheng, H. T.; Astruc, D.; Zhu, M. Z., Atomically precise noble metal nanoclusters as efficient catalysts: A bridge between structure and properties. *Chem. Rev.* **2020,** *120*, 526-622.
11. Lee, K.; Kim, M.; Kim, H., Catalytic nanoparticles being facet-controlled. *J. Mater. Chem.* **2010,** *20*, 3791-3798.
12. Pal, J.; Pal, T., Faceted metal and metal oxide nanoparticles: design, fabrication and catalysis. *Nanoscale* **2015,** *7*, 14159-14190.
13. Xie, C. L.; Niu, Z. Q.; Kim, D.; Li, M. F.; Yang, P. D., Surface and interface control in nanoparticle catalysis. *Chem. Rev.* **2020,** *120*, 1184-1249.
14. Mistry, H.; Varela, A. S.; Kuhl, S.; Strasser, P.; Cuenya, B. R., Nanostructured electrocatalysts with tunable activity and selectivity. *Nat. Rev. Mater.* **2016,** *1*, 16009.
15. Gan, L.; Heggen, M.; O'Malley, R.; Theobald, B.; Strasser, P., Understanding and controlling nanoporosity formation for improving the stability of bimetallic fuel cell catalysts. *Nano Lett.* **2013,** *13*, 1131-1138.
16. Wronski, C. R. M., The size dependence of the melting point of small particles of tin. *Br. J. Appl. Phys.* **1967,** *18*, 1731.
17. Allen, G. L.; Bayles, R. A.; Gile, W. W.; Jesser, W. A., Small particle melting of pure metals. *Thin solid films* **1986,** *144*, 297-308.
18. Sambles, J. R., An electron microscope study of evaporating gold particles: the Kelvin equation for liquid gold and the lowering of the melting point of solid gold particles. *Proc. Royal Soc. London. A. Mathemat. Phys. Sci.* **1971,** *324*, 339-351.
19. Johny, J.; Prymak, O.; Kamp, M.; Calvo, F.; Kim, S. H.; Tymoczko, A.; El-Zoka, A.; Rehbock, C.; Schürmann, U.; Gault, B.; Kienle, L.; Barcikowski, S., Multidimensional thermally-induced transformation of nest-structured complex Au-Fe nanoalloys towards equilibrium. *Nano Res.* **2022,** *15*, 581-592.
20. Pappert, K.; Loza, K.; Shviro, M.; Hagemann, U.; Heggen, M.; Dunin-Borkowski, R. E.; Schierholz, R.; Maeda, T.; Kaneko, K.; Epple, M., Nanoscopic porous iridium/iridium dioxide superstructures (15 nm): Synthesis and thermal conversion by in situ transmission electron microscopy. *Chem. Eur. J.* **2019,** *25*, 11048-11057.
21. Vara, M.; Wang, X.; Howe, J.; Chi, M. F.; Xia, Y. N., Understanding the stability of Pt-based nanocages under thermal stress using in situ electron microscopy. *ChemNanoMat* **2018,** *4*, 112-117.
22. Li, J.; Wang, Z.; Li, Y.; Deepak, F. L., In situ atomic-scale observation of kinetic pathways of sublimation in silver nanoparticles. *Adv. Sci.* **2019,** *6*, 1802131.
23. Asoro, M. A.; Kovar, D.; Ferreira, P. J., In situ transmission electron microscopy observations of sublimation in silver nanoparticles. *ACS Nano* **2013,** *7*, 7844-7852.
24. Ding, Y.; Fan, F. R.; Tian, Z. Q.; Wang, Z. L., Sublimation-induced shape evolution of silver cubes. *Small* **2009,** *5*, 2812-2815.
25. Guisbiers, G.; Mendoza-Cruz, R.; Bazan-Diaz, L.; Velazquez-Salazar, J. J.; Mendoza-Perez, R.; Robledo-Torres, J. A.; Rodriguez-Lopez, J. L.; Montejano-Carrizales, J. M.; Whetten, R. L.; Jose-Yacaman, M., Electrum, the gold–silver alloy, from the bulk scale to the nanoscale: synthesis, properties, and segregation rules. *ACS Nano* **2016,** *10*, 188-198.

26. Im, S. H.; Lee, Y. T.; Wiley, B.; Xia, Y., Large-scale synthesis of silver nanocubes: the role of HCl in promoting cube perfection and monodispersity. *Angew. Chem. Int. Ed.* **2005,** *44*, 2154-2157.
27. Helmlinger, J.; Prymak, O.; Loza, K.; Gocyla, M.; Heggen, M.; Epple, M., On the crystallography of silver nanoparticles with different shapes. *Cryst. Growth Des.* **2016,** *16*, 3677-3687.
28. Skrabalak, S. E.; Au, L.; Li, X. D.; Xia, Y. N., Facile synthesis of Ag nanocubes and Au nanocages. *Nat. Protoc.* **2007,** *2*, 2182-2190.
29. Sun, Y. G.; Xia, Y. N., Shape-controlled synthesis of gold and silver nanoparticles. *Science* **2002,** *298*, 2176-2179.
30. Loza, K.; Diendorf, J.; Greulich, C.; Ruiz-Gonzales, L.; Gonzalez-Calbet, J. M.; Vallet-Regi, M.; Koeller, M.; Epple, M., The dissolution and biological effect of silver nanoparticles in biological media. *J. Mater. Chem. B* **2014,** *2*, 1634-1643.
31. Thust, A.; Barthel, J.; Tillmann, K., FEI Titan 80-300 TEM. *J. Large-scale Res. Fac.* **2016,** *2*, A41.
32. Wang, B.; Zhang, L.; Zhou, X., Synthesis of silver nanocubes as a SERS substrate for the determination of pesticide paraoxon and thiram. *Spectrochim. Acta A: Mol. Biomol. Spectrosc.* **2014,** *121*, 63-69.
33. Wang, H. S.; Qiao, X. L.; Chen, J. G.; Ding, S. Y., Preparation of silver nanoparticles by chemical reduction method. *Colloid Surf. A-Physicochem. Eng. Asp.* **2005,** *256*, 111-115.
34. Zhou, F.; Li, Z. Y.; Liu, Y.; Xia, Y., Quantitative analysis of dipole and quadrupole excitation in the surface plasmon resonance of metal nanoparticles. *J. Phys. Chem. C* **2008,** *112*, 20233-20240.
35. Martinez, J. C.; Chequer, N. A.; Gonzalez, J. L.; Cordova, T., Alternative methodology for gold nanoparticles diameter characterization using PCA technique and UV-VIS spectrophotometry. *Nanosci. Nanotechnol.* **2012,** *2*, 184-189.
36. Alpay, D.; Peng, L.; Marks, L. D., Are nanoparticle corners round? *J. Phys. Chem. C* **2015,** *119*, 21018-21023.
37. Wang, G.; Liu, Y.; Gao, C.; Guo, L.; Chi, M.; Ijiro, K.; Maeda, M.; Yin, Y., Island growth in the seed-mediated overgrowth of monometallic colloidal nanostructures. *Chem* **2017,** *3*, 678-690.
38. Banerjee, S.; Loza, K.; Meyer-Zaika, W.; Prymak, O.; Epple, M., Structural evolution of silver nanoparticles during wet-chemical synthesis. *Chem. Mater.* **2014,** *26*, 951-957.
39. Nanda, K. K.; Maisels, A.; Kruis, F. E.; Rellinghaus, B., Anomalous thermal behavior of gold nanostructures. *Europhys. Lett.* **2007,** *80*, 56003.
40. Rahman, T.; McCloy, J.; Ramana, C. V.; Panat, R., Structure, electrical characteristics, and high-temperature stability of aerosol jet printed silver nanoparticle films. *J. Appl. Phys.* **2016,** *120*, 075305.
41. Prymak, O.; Grasmik, V.; Loza, K.; Heggen, M.; Epple, M., Temperature-induced stress relaxation in alloyed silver–gold nanoparticles (7–8 nm) by in situ x-ray powder diffraction. *Cryst. Growth Des.* **2020,** *20*, 107-115.
42. Tomizuka, C. T.; Sonder, E., Self-diffusion in silver. *Phys. Rev.* **1956,** *103*, 1182-1184.
43. Swanson, H. E.; Tatge, E., Standard x-ray diffraction patterns. *J. Res. Natl. Bur. Stand.* **1951,** *46*, 318-327.

44. Prymak, O.; Jakobi, J.; Rehbock, C.; Epple, M.; Barcikowski, S., Crystallographic characterization of laser-generated, polymer-stabilized 4 nm silver-gold alloyed nanoparticles. *Mater. Chem. Phys.* **2018,** *207*, 442-450.
45. Schadel, H. M.; Birchenall, C. E., The vapor pressure of silver. *JOM* **1950,** *2*, 1134-1138.
46. Chatterjee, B., Anisotropy of melting for cubic metals. *Nature* **1978,** *275*, 203-203.
47. Bembel, A. G., On the size dependences of the metallic nanoparticle evaporation and sublimation heats: thermodynamics and atomistic modeling. *Russ. Phys. J.* **2017,** *59*, 1567-1574.